FIRST RESULTS FROM THE ATLAS EXPERIMENT ON PRODUCTION OF W AND Z BOSONS IN PROTON–PROTON COLLISIONS AT $\sqrt{s} = 7$ TeV*

Paweł Malecki

on behalf of the ATLAS Collaboration

The Henryk Niewodniczański Institute of Nuclear Physics
Polish Academy of Sciences
Radzikowskiego 152, 31-342 Kraków, Poland

(Received April 29, 2011)

First results for the W and Z boson production cross-sections at $\sqrt{s} =$ 7 TeV obtained with the ATLAS detector are presented. The measurements are performed in electron and muon channels, with a data sample of around 320 nb^{-1} collected between March and July 2010. Methods of signal extraction and background estimation are briefly presented. The measured values of W production cross-sections in electron and muon channels are $\sigma_W \times \mathrm{BR}(W \to e\nu) = 10.51 \pm 1.45$ nb and $\sigma_W \times \mathrm{BR}(W \to \mu\nu) = 9.58 \pm 1.20$ nb. The Z cross-section measurements yield $\sigma_Z \times \mathrm{BR}(Z \to ee) = 0.75 \pm 0.14$ nb and $\sigma_Z \times \mathrm{BR}(Z \to \mu\mu) = 0.87 \pm 0.14$ nb. The obtained results are in good agreement with theoretical predictions. A preliminary measurement of the W boson charge asymmetry is also presented.

DOI:10.5506/APhysPolB.42.1505
PACS numbers: 13.38.Be, 13.38.Dg, 13.40.Hq

1. Introduction

A very important point in the ATLAS program of first physics measurements is the observation of W and Z bosons and their properties. Theoretical predictions for W/Z production cross-sections are nowadays very precise [1], so a fine measurement is needed to test these predictions, which are sensitive to higher-order (NNLO) QCD corrections as well as Parton Distribution Functions (PDF) of the proton [2]. New constraints on the latter are expected to be obtained with LHC measurements of W and Z bosons. In addition, these bosons as first sources of high-transverse-momentum isolated leptons are important for detector and algorithm commissioning.

* Presented at the Cracow Epiphany Conference on the First Year of the LHC, Cracow, Poland, January 10–12, 2011.

The existence of W and Z bosons has been first proposed by Glashow, Weinberg and Salam in the 1960s [3]. After their discovery by the UA1 and UA2 experiments at the Super Proton Synchrotron (SPS) at CERN [4] in proton–antiproton collisions, their properties have been thoroughly measured at LEP, SLC, RHIC and Tevatron, at different center-of-mass energies varying from $\sqrt{s} = 500$ GeV up to $\sqrt{s} = 1.96$ TeV. Further confirmation of previous results, improved accuracy and extension of the measurements into previously unexplored kinematic domains are the current goals for LHC experiments.

The studies presented here are based on electron and muon final states, either in a lepton–neutrino pair or in two oppositely charged leptons. This ensures a clean experimental signature based on high-p_{T} isolated charged leptons, which can be easily identified and separated from the background dominated by QCD processes. The following analyses have been published by the ATLAS Collaboration in [5].

2. The ATLAS detector

The ATLAS detector [6] is the largest of the four detectors at the Large Hadron Collider (LHC) and one of two so-called general-purpose detectors, designed for most precision measurements, including Standard Model (SM) tests, Higgs boson searches, SUSY searches, but also aspects of B physics and Heavy Ion collisions. It provides almost full solid-angle coverage around the beam crossing point and allows for detailed and precise studies of collision events.

In the ATLAS coordinate system the z-axis is parallel to the beam-line and points towards the anti-clockwise direction of the beam in LHC ring. The x-axis points towards the ring center, setting the $\phi = 0$ value of the azimuthal angle and the y-axis points upwards. The transverse quantities (like transverse momentum, p_{T}, or missing transverse energy, $E_{\mathrm{T}}^{\mathrm{Miss}}$) are defined in the x–y plane.

The detector is built of concentric layers around the beam-line. The innermost subsystem is responsible for tracking of charged particles. It is immersed in a 2 T axial magnetic field parallel to the beam-line. Further layers consist of calorimeters and muon chambers. The muon system has its own toroidal magnetic field surrounding the detector. The Inner Detector (ID) provides coverage over full azimuthal angle and pseudorapidity within $|\eta| < 2.47$. It consists of three subsystems, the two innermost being silicon detectors, namely the Pixel and Semiconductor Tracker (SCT), and the outer being the gaseous Transition Radiation Tracker (TRT). The calorimeters surround the ID and solenoid magnet and cover up to $|\eta| < 4.9$. Liquid Argon (LAr) and scintillating tiles are used as active media, with lead and steel being the respective absorber material. The calorimeters are

segmented, both longitudinally and transversely, to allow for shower-shape studies, useful for particle identification. The electromagnetic (EM) part of the ATLAS calorimeter system has a depth of at least 22 radiation-lengths, whereas the hadronic part is approximately 10 interaction lengths deep. The Muon Spectrometer (MS) provides the possibility to measure muon tracks within $|\eta| < 2.7$. Tracking capabilities in the MS are assured by drift tube detectors and cathode-strip chambers.

3. Data samples and Monte Carlo simulations

The presented analysis is based on the data sample collected by ATLAS between March and July 2010. It corresponds to an integrated luminosity of approximately 310–331 nb^{-1} (depending on the channel). For the electron channel, the sample was selected by a Level-1 calorimetric trigger, requiring an electromagnetic cluster with transverse energy $E_{\text{T}} > 10$ GeV. Muon events were selected by comparing the signal pattern from the Muon Spectrometer with reference tables based on muon tracks, starting at an effective p_{T} threshold of 6 GeV.

Monte Carlo samples were generated by PYTHIA [7] using MRSTLO* [2] Parton Distribution Functions. Detector simulation [8] is performed by the GEANT4 [9] package.

4. Object reconstruction

4.1. Electrons

The reconstruction of electrons in ATLAS is based on electromagnetic clusters in the calorimeter. Such a cluster is matched to a track reconstructed in the Inner Detector. The matched candidate object subsequently undergoes the identification procedure, based on cuts applied on electromagnetic shower shapes (both longitudinal and transverse), track quality and the actual distance (in η–ϕ) between track and cluster. Three sets of selection criteria are used as a reference, namely the *Loose*, *Medium* and *Tight* cuts. They provide strongly increasing rejection power against the background, with a small decrease of signal efficiency. *Loose* criteria are based on the energy deposits in the second layer of electromagnetic calorimeter, *Medium* ones add more restrictive criteria on the shower shape in the first layer and on track-quality variables. The *Tight* requirements, in addition to even tighter track selection and shower-shape restrictions reject electrons from photon conversions.

4.2. Muons

In this analysis the *combined* muon objects are considered. They utilize the information from both the Muon Spectrometer and Inner Detector. The

association between the tracks from these two subsystems is performed using a χ^2 test comparing the differences between track parameters weighted by their covariance matrices.

4.3. Missing transverse energy

To account for a neutrino that appears in $W \to \ell\nu$ and is not reconstructed, a missing transverse energy ($E_{\mathrm{T}}^{\mathrm{Miss}}$) is calculated, based on calorimeter information. A vector sum of energy deposits in cells that belong to reconstructed clusters is calculated in both x and y directions, and then combined into $E_{\mathrm{T}}^{\mathrm{Miss}}$. This is an important tool to discriminate against QCD background in $W \to \ell\nu$ signal extraction procedures. In these studies, the missing transverse energy is reconstructed assuming all energy is deposited by electromagnetic processes, and then corrected for different calorimeter response for hadrons. In the analysis of the muon channel, the missing transverse energy is corrected for the muon momentum.

5. Event selection

5.1. Preselection of high-p_{T} leptons

Data samples containing high transverse momentum leptons are first selected from the datasets available after trigger filtering. The lepton candidate is required to be contained within detector acceptance. In the case of electrons the region $|\eta| < 2.47$ is considered (being the coverage of Inner Detector) with the exception of $1.37 < |\eta| < 1.52$ barrel — end-cap transition regions in the calorimeter. The acceptance region for muons is defined

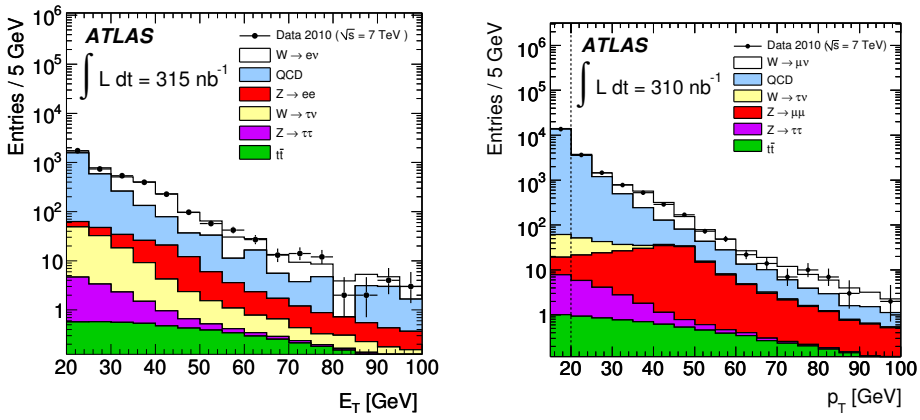

Fig. 1. Left: Spectrum of calorimeter cluster E_{T} of electron candidates after *tight* selection. Right: Transverse momentum of muon candidates. In both channels data and Monte Carlo are compared with the simulated sample broken down into various signal and background contributions.

as $|\eta| < 2.4$. In addition, the electron cluster transverse energy is required to be $E_{\mathrm{T}} > 20$ GeV, and the muon transverse momentum needs to satisfy $p_{\mathrm{T}} > 20$ GeV.

The selected samples are further refined by adding requirements on leptons. The electrons selected for $W \to e\nu$ analysis need to pass the *tight* identification criteria, whereas *medium* cuts are applied in $Z \to ee$ selection. In $Z \to \mu\mu$ and $W \to \mu\nu$ selections, lepton isolation criteria are exploited. The sum of transverse momenta of tracks surrounding the candidate in the cone of $\Delta R < 0.4$ must not exceed 20% of the muon candidate transverse momentum. Fig. 1 shows the spectra of E_{T} and p_{T} of *tight* electrons and muons respectively, with data and various Monte Carlo-based contributions. Further selection procedure and background suppression is needed and is based on event topologies.

5.2. Selection of $W \to \ell\nu$ sample

In addition to a high-p_{T} lepton, transverse missing energy is present in $W \to \ell\nu$ events, accounting for a neutrino escaping detection. A cut of $E_{\mathrm{T}}^{\mathrm{Miss}} > 25$ GeV is applied in both channels. A transverse mass of W boson, defined as

$$m_{\mathrm{T}} = \sqrt{2p_{\mathrm{T}}^{\ell} E_{\mathrm{T}}^{\mathrm{Miss}} \left[1 - \cos\left(\phi^{\ell} - \phi^{E_{\mathrm{T}}^{\mathrm{Miss}}\ 0}\right)\right]}$$

is also reconstructed, and a cut of $m_{\mathrm{T}} > 40$ GeV is applied. Spectra of transverse missing energy and transverse mass in both channels are presented in Fig. 2. Clearly, the cuts mentioned above are crucial to reduce the overall background rate.

The final number of events that fulfill the final selection criteria is found to be 1069 in the electron channel and 1181 in the muon channel. The contributions of various processes to these samples will be discussed in Sec. 6.

5.3. $Z \to \ell\ell$ event selection

The selection of $Z \to \ell\ell$ events imposes a requirement of the presence of two oppositely-charged leptons, either *medium* electrons, or muons. In addition, only events with a lepton–lepton system invariant mass window of $66 < m_{\ell\ell} < 116$ GeV are considered. Events containing more than two leptons passing selection requirements are vetoed. Figure 3 shows the distributions of Z-boson invariant mass in each channel. Discrepancies between the shapes obtained from data and Monte Carlo predictions were investigated and result from detector misalignments and imperfect description of magnetic field. The total number of data events passing the Z selection is 70 and 109 in the electron and muon channels respectively. Background contributions for this dilepton selection are discussed in Sec. 6.

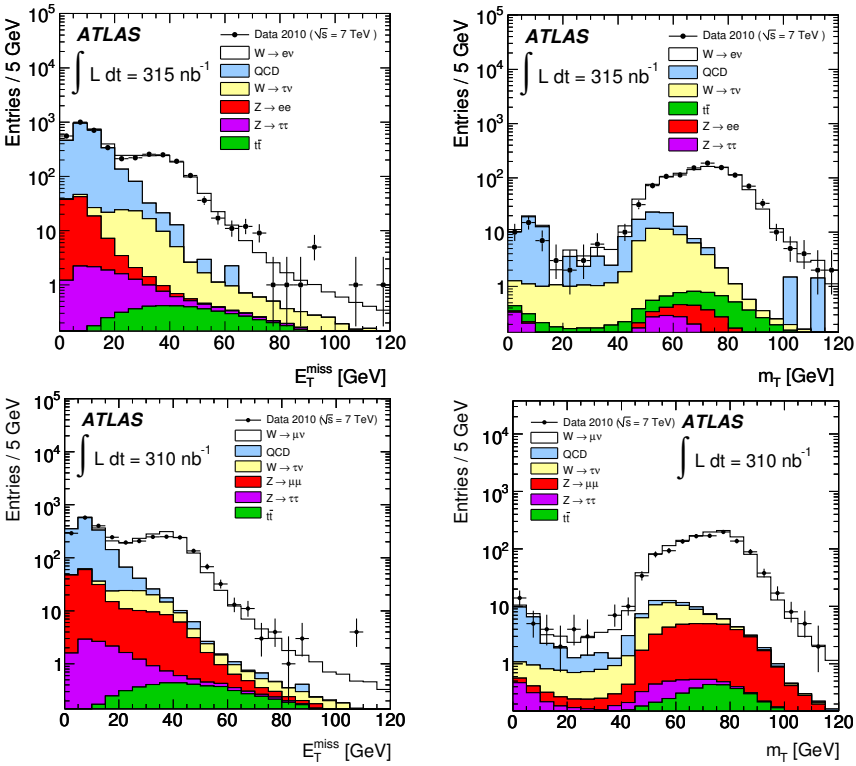

Fig. 2. Top row: electron channel, bottom: muon channel. Left: Transverse missing energy in the electron (muon) channel after *tight* electron (isolated muon) selection, Right: Transverse mass after $E_{\mathrm{T}}^{\mathrm{Miss}}$ cut. In each plot data and Monte Carlo samples are shown, with the latter broken down into various signal and background components.

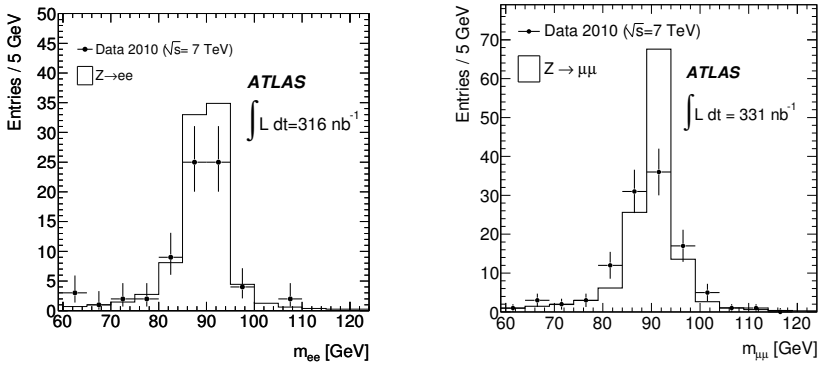

Fig. 3. Invariant mass of Z boson in electron (left) and muon (right) channels.

6. Background estimation

In each signal channel two classes of background processes are under consideration, namely the *non-QCD* (sometimes referred to as *electroweak*) processes, including decays of W and Z bosons different from the intended signal, and the QCD di-jet background. The contribution from the former class to the final signal sample is estimated from Monte Carlo simulations, as these processes are well-modeled at NLO and NNLO, and the associated uncertainty on number of background events is therefore small. The contribution from the latter needs however to be estimated with data-driven methods (with the exception of the $Z \to \mu\mu$ process), as the associated uncertainty on the current (LO) Monte Carlo estimations is more than 100%. A summary of the background contributions to the described channels is given in Table I.

TABLE I

Number of selected events and background expectations for the processes under consideration.

Process	Lumi	No. of evets	Non-QCD bkg.	QCD bkg.
$W \to e\nu$	315 nb^{-1}	1069	$33.5 \pm 0.2 \pm 3.0$	$28 \pm 3 \pm 10$
$W \to \mu\nu$	310 nb^{-1}	1181	$77.6 \pm 0.3 \pm 5.4$	$23 \pm 5 \pm 9$
$Z \to ee$	316 nb^{-1}	70	$0.27 \pm 0.0 \pm 0.03$	$0.9 \pm 0.1 \pm 0.4$
$Z \to \mu\mu$	331 nb^{-1}	109	$0.21 \pm 0.01 \pm 0.01$	$0.04 \pm 0.01 \pm 0.04$

6.1. Backgrounds for $W \to \ell\nu$

The contribution of non-QCD background to this channel has been assessed with Monte Carlo samples. $W \to \tau\nu$ and $Z \to \ell\ell$ decays are under consideration, as well as the $t\bar{t}$ process. In the electron channel, the most significant non-QCD background process is $W \to \tau\nu$ with τ decaying into an electron and a pair of neutrinos, constituting 77% of the non-QCD background. In the muon channel, the $Z \to \mu\mu$ events are the most numerous (49%) among electroweak backgrounds.

The number of QCD background events in electron channel selection is assessed with a fit of signal and background templates to the $E_{\mathrm{T}}^{\mathrm{Miss}}$ distribution. The shape of the templates is either obtained from simulations (in the case of $W \to \ell\nu$ signal) or determined with data-driven methods involving reversal of certain electron identification cuts and rejecting events with isolated leptons. Results of this fit are shown in Fig. 4. The number of events estimated with this method is 28 ± 3(stat.)± 10(syst.), with systematic uncertainties obtained by varying the fit range and the cuts for template extraction.

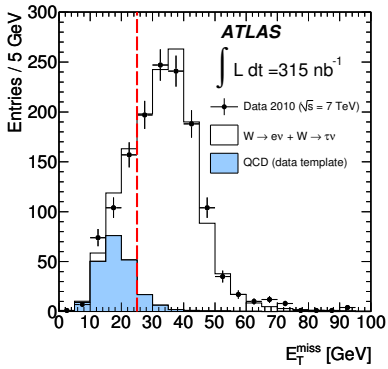

Fig. 4. Result of $E_{\mathrm{T}}^{\mathrm{Miss}}$ template fits in number of QCD background events estimation.

In the muon channel, the number of QCD events with high missing transverse energy and well-isolated muons is estimated with the knowledge of muon-isolation criteria efficiency measured with $Z \to \mu\mu$ events, and from background-dominated low-p_{T} muon sample. The estimate gives $23 \pm 5(\mathrm{stat.}) \pm 9(\mathrm{syst.})$ events, with a systematic uncertainty dominated by the uncertainty on the isolation efficiency for QCD events.

6.2. $Z \to \ell\ell$ background estimation

Even though the number of $Z \to \ell\ell$ events is much less than the number of $W \to \ell\nu$ events, the background contributions are also much lower, resulting in cleaner samples after event selection. The total number of non-QCD background events in the considered mass window of $66 < m_{\ell\ell} < 116$ GeV is $0.27 \pm 0.00(\mathrm{stat.}) \pm 0.03(\mathrm{syst.})$ in the electron channel and $0.21 \pm 0.01(\mathrm{stat.}) \pm 0.01(\mathrm{syst.})$ in the muon channel.

The QCD background for the $Z \to ee$ process is estimated from data. Electron identification requirements are relaxed from *medium* to *loose*, and a fit of a Breit–Wigner function convoluted with a Gaussian one (modelling the signal) and a second-order polynomial (describing the background) is performed in a broader range of invariant mass. The resulting number of background events is then scaled down by a rejection factor matching the *medium* electron identification performance, derived from data. The final estimate is $0.91 \pm 0.11(\mathrm{stat.}) \pm 0.41(\mathrm{syst.})$ events. The systematic uncertainty is estimated by varying the electron identification criteria, changing bin sizes and replacing the second-order polynomial in the fit with a first-order one.

In the muon channel, the QCD background is also assessed with Monte Carlo simulations. Background contributions from heavy quark decays are estimated to be 0.04 events with a statistical uncertainty of 0.01. The systematic error on Monte Carlo rates is large, and it is conservatively assigned to be 100% in this study.

7. Acceptances and efficiencies

The acceptance and efficiency factors are needed for the cross-section measurements presented in Sec. 8. They describe the kinematic and geometrical acceptance of the detector and selection procedures, as well as discrepancies between truth-level and detector-level selection. The acceptance ($A_{W/Z}$) is calculated from PYTHIA generator-level quantities. The selection efficiency ($C_{W/Z}$) is, in these studies, also obtained from Monte Carlo (reconstruction-level quantities), but in further analyses with larger datasets most of its components will be measured from data. A summary on acceptance and efficiency factors is given in Table II.

TABLE II

Acceptances and efficiencies for the considered signal channels.

Process	Acceptance ($A_{W/Z}$)	Efficiency ($C_{W/Z}$)
$W \to e\nu$	0.462 ± 0.014	0.659 ± 0.046
$W \to \mu\nu$	0.480 ± 0.014	0.758 ± 0.030
$Z \to ee$	0.446 ± 0.018	0.651 ± 0.061
$Z \to \mu\mu$	0.486 ± 0.019	0.773 ± 0.038

7.1. W acceptance and selection efficiency

The $W \to \ell\nu$ acceptance is obtained by applying the following cuts at truth (generator) level: $p_{\mathrm{T}}^{\ell} > 20$ GeV, $p_{\mathrm{T}}^{\nu} > 25$ GeV. Pseudorapidity regions of $|\eta^e| < 2.47$ without $1.37 < |\eta^e| < 1.52$ or $|\eta^\mu| < 2.4$ are considered. A cut on $m_{\mathrm{T}} > 40$ GeV is also applied. The systematic uncertainty of 3% for each channel results from discrepancies in Monte Carlo models of PYTHIA and MC@NLO [10] and also from differences in the PDF sets.

The efficiency of the $W \to \ell\nu$ selection describes the influence of truth-level *versus* detector-level discrepancies and consists of trigger and event reconstruction efficiencies, as well as the performance of lepton selection and energy scale resolution. The total systematic uncertainty on C_W is 7% in the electron channel and 4% in the muon channel.

7.2. Z acceptance and selection efficiency

Similarly the acceptance for $Z \to \ell\ell$ is obtained, by requiring (at truth level) the presence of two leptons with $p_{\mathrm{T}}^{\ell} > 20$ GeV. Pseudorapidity range of $|\eta^e| < 2.47$ without the region of $1.37 < |\eta^e| < 1.52$ or $|\eta^\mu| < 2.4$ is considered. The events are required to lie within an invariant mass window of $66 < m_{\ell\ell} < 116$ GeV. A 3% systematic error is assigned to account for PDF uncertainties and discrepancies between calculations at NLO and NNLO.

The selection efficiency factor C_Z contains dominant factors from lepton selection and trigger efficiencies, both of which are squared to account for two charged leptons that need to be observed in such events. Its systematic uncertainty on C_Z is 9.4% and 5.5% in the electron and muon channels, respectively.

8. Cross-section measurement

The cross-section for W/Z production times the branching fraction of considered decay modes are expressed as follows:

$$\sigma_{W(Z)} \times \mathrm{BR}(W(Z) \to \ell\nu(\ell\ell)) = \frac{N_{\mathrm{obs}} - N_{\mathrm{bkg}}}{A_{W(Z)} C_{W(Z)} L_{\mathrm{int}}} . \tag{1}$$

The components of the right-hand side of Eq. (1) have been presented in the previous sections. N_{obs} is the number of observed events in each channel, N_{bkg} denotes the estimated number of background events, and $A_{W(Z)}$ and $C_{W(Z)}$ stand for event acceptance and selection efficiency, respectively. L_{int} is the total integrated luminosity of each sample. Results of this calculation are presented in Table III. The dominant contribution to the uncertainty results from the luminosity measurement error of 11%.

TABLE III

Cross-section values measured in each described channel.

Process	Cross-section times branching fraction [nb]
$W \to e\nu$	$10.51 \pm 0.34(\mathrm{stat.}) \pm 0.81(\mathrm{syst.}) \pm 1.16(\mathrm{lum})$
$W \to \mu\nu$	$9.58 \pm 0.30(\mathrm{stat.}) \pm 0.50(\mathrm{syst.}) \pm 1.05(\mathrm{lum})$
$Z \to ee$	$0.75 \pm 0.09(\mathrm{stat.}) \pm 0.08(\mathrm{syst.}) \pm 0.08(\mathrm{lum})$
$Z \to \mu\mu$	$0.87 \pm 0.08(\mathrm{stat.}) \pm 0.06(\mathrm{syst.}) \pm 0.10(\mathrm{lum})$

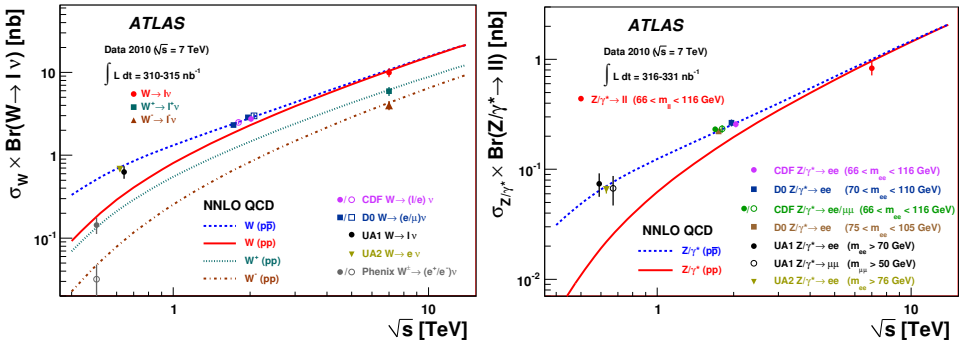

Fig. 5. Cross-section measurement results in context of results from previous experiments and Monte Carlo predictions. Left: $W \to \ell\nu$, right: $Z \to \ell\ell$.

The obtained results of cross-section measurements are in good agreement with the theoretical predictions for W and Z production at NNLO, which are 10.46 ± 0.52 nb and 0.96 ± 0.05 nb, respectively. Figure 5 shows the obtained results in the context of Monte Carlo predictions and previous measurements from PHENIX (pp collisions), UA1, UA2, CDF and D0 experiments ($p\bar{p}$ collisions).

9. W charge asymmetry

In LHC proton–proton collisions an asymmetry between the numbers of positively and negatively charged W bosons is expected. This is not seen in charge-symmetric proton–antiproton collisions at SPS or Tevatron. This asymmetry depends on the fractions of momenta carried by each colliding parton, and therefore the ratio of W^+ to W^- bosons should depend on pseudorapidity.

The W charge asymmetry is measured with the following quantity A

$$A = \frac{\sigma_{\text{fid}}\,(W^+) - \sigma_{\text{fid}}\,(W^-)}{\sigma_{\text{fid}}\,(W^+) + \sigma_{\text{fid}}\,(W^-)}\,. \tag{2}$$

In the definition above, $\sigma_{\text{fid}}(W^{\pm})$ is the so-called *fiducial* cross-section, measured by assuming the acceptance equal to 1.0. This reduces the possible bias from theoretical predictions on this measurement.

Results of this measurement are presented in Fig. 6. The data sample used for this measurement is the same as for the measurement of W cross-section described in previous sections. Good agreement with theoretical predictions is obtained with the current statistical sensitivity.

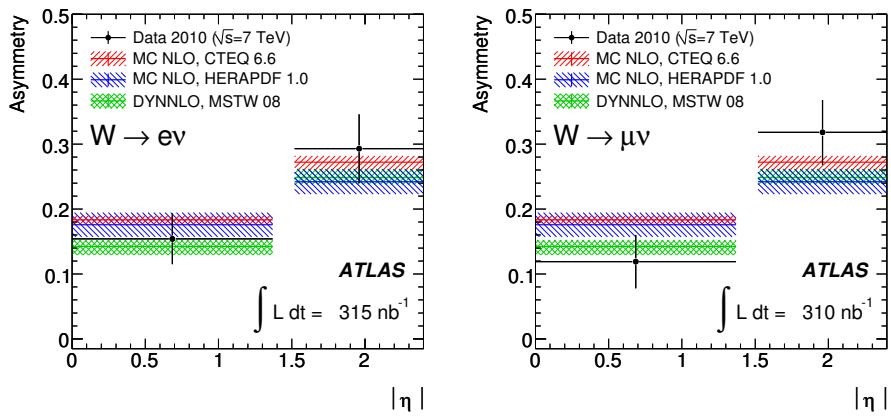

Fig. 6. W charge asymmetry with respect to pseudorapidity in electron (left) and muon (right) channels. The error bands show the theoretical uncertainties obtained with PDF error eigenvector set at 90% C.L.

10. Summary

The ATLAS experiment has observed the first W and Z bosons at the center-of-mass energy of 7 TeV. The production cross-sections of these bosons have been measured in both electron and muon decay channels yielding results that are in good agreement with theoretical Standard Model predictions. The W charge asymmetry has also been measured to be consistent with Monte Carlo predictions. The presented paper summarizes the results published by the Collaboration in [5]. This analysis will be updated with the full 2010 data, and a large reduction of both statistical and systematic uncertainty is expected, including reduced luminosity uncertainty and error on selection efficiencies.

REFERENCES

[1] K. Melnikov, F. Petriello, *Phys. Rev.* **D74**, 114017 (2006).

[2] A. Martin, R. Roberts, J. Stirling, R. Thorne, *Eur. Phys. J.* **C14**, 133 (2000) [arXiv:hep-ph/9907231v1].

[3] S. Glashow, *Nucl. Phys.* **22**, 579 (1961); S. Weinberg, *Phys. Rev. Lett.* **19**, 1264 (1967); A. Salam, Gauge Unification of Fundamental Forces, Nobel lecture, Dec 8, 1979.

[4] G. Arnison *et al.* [UA1 Collaboration], *Phys. Lett.* **B122**, 103 (1983); M. Banner *et al.* [UA2 Collaboration], *Phys. Lett.* **B122**, 476 (1983); G. Arnison *et al.* [UA1 Collaboration], *Phys. Lett.* **B126**, 398 (1983); P. Baganaia *et al.* [UA2 Collaboration], *Phys. Lett.* **B129**, 130 (1983).

[5] [ATLAS Collaboration], *J. High Energy Phys.* **1012**, 060 (2010) [arXiv:1010.2130v1 [hep-ex]].

[6] [ATLAS Collaboration], *JINST* **3**, S08003 (2008).

[7] T. Sjostrand, S. Mrenna, P. Skands, *J. High Energy Phys.* **05**, 026 (2006).

[8] [ATLAS Collaboration], *Eur. Phys. J.* **C70**, 823 (2010) [arXiv:1005.4568 [physics.ins-det]].

[9] S. Agostinelli *et al.* [GEANT4 Collaboration], *Nucl. Instrum. Methods* **A506**, 250 (2003).

[10] S. Frixione, P. Nason, B.R. Webber, *J. High Energy Phys.* **0308**, 007 (2003).